Eur. Phys. J. A (2023) 59:117
https://doi.org/10.1140/epja/s10050-023-01026-3

THE EUROPEAN PHYSICAL JOURNAL A

Regular Article - Experimental Physics

Advances in nuclear structure via charged particle reactions with AGATA

D. Mengoni[1,2,a], D. Beaumel[3], W. N. Catford[4], M. Assié[3], D. Brugnara[1,5], F. Galtarossa[2], A. Gottardo[5], I. Zanon[5,6], M. Zielińska[7]

[1] Dipartimento di Fisica e Astronomia, Università di Padova, via F. Marzolo, 8-35131 Padova, Italy
[2] INFN Sezione di Padova, via F. Marzolo, 8-35131 Padova, Italy
[3] Université Paris-Saclay, CNRS/IN2P3, IJCLab, 91405 Orsay, France
[4] Department of Physics, University of Surrey, Guildford GU2 7XH, UK
[5] INFN Laboratori Nazionali di Legnaro, Legnaro, Italy
[6] Dipartimento di Fisica e Scienze della Terra, Università di Ferrara, via G. Saragat, 1-44122 Ferrara, Italy
[7] Irfu, CEA, Université Paris-Saclay, 91191 Gif-sur-Yvette, France

Received: 19 March 2023 / Accepted: 6 May 2023

Communicated by Nicolas Alamanos

Abstract In recent decades, γ-ray spectroscopy has undergone a major technological leap forward, namely the technique of γ-ray tracking, and has attained a sensitivity that is two orders of magnitude larger than that provided by the former generation of Compton-shielded arrays. Indeed the gain is comparable with the achievements since the dawn of γ-ray spectroscopy. Such sensitivity can be further heightened by coupling γ-ray spectrometers to other detectors that record complementary reaction products such as light-charged particles for transfer reactions and scattered ions for Coulomb excitation measurements. Nucleon transfer reactions offer an excellent mean to probe the energies of shell model single-particle orbitals and to study migration in energy of these orbitals as we venture away from stability. Such measurements can also estimate the cross sections of processes relevant to stellar evolution and nucleosynthesis. The measurement of γ rays in coincidence with particles provides also information on the decay channel for unbound systems, which constitutes a useful input for astrophysics and nuclear structure near the drip-lines. Coulomb-excitation studies make it possible to infer collective structure in nuclei and to extract deformation properties of, in particular, open-shell systems. Here, selected examples will be presented, highlighting the power of these types of experiments when γ-ray observation is included. The development of the experimental methods is reviewed, showing the results achieved before the advent of γ-ray tracking. Examples of more recent experiments that have successfully exploited γ-ray tracking with AGATA are then presented as showcases for the outstanding performance of the composite detection systems. The outlook for experiments using newly developed devices such as GRIT and other detectors such as SPIDER is described.

1 Introduction

Single-nucleon transfer reactions provide a powerful experimental tool to selectively populate the nuclear states of interest. These states have a structure that is given by the original nucleus as a core, with the transferred nucleon in an orbit around it. Nucleon transfer is thus an excellent way to probe the energies of shell model orbitals and to study the changes in the energies of these orbitals as we venture away from stability.

Traditionally, for a nucleon transfer reaction such as (d, p) or (p, d) or (d, t), the emphasis has been primarily on measuring the light ejectiles, the protons or deuterons or tritons. This is because the energy of the proton in a (d, p) reaction, for example, gives information about which state in the final nucleus is populated. Further, the angular distribution is characteristic of the angular momentum transferred to the target nucleus by the nucleon. The combination of energy and angular momentum distribution enable the reconstruction of the level scheme that can be then compared with theoretical models. At a practical level, if the transfer takes place upon a short-lived radioactive nucleus, it must be performed with the radioactive species as the projectile and with a light nucleus (p, d, t, ^{3}He, ^{4}He, ^{6,7}Li) as the target, a situation known as inverse kinematics. This generally means that the resolution

[a] e-mail: daniele.mengoni@pd.infn.it (corresponding author)

Published online: 26 May 2023

in excitation energy (based upon the energies and angles of the emitted protons from (d, p) for example) could be much worse than required due to the target thickness. Gamma-ray measurements can solve this problem.

Thus, there are two very important reasons for measuring γ rays, as well as particles, in transfer: allowing different excited states to be distinguished using precise energy measurements when they are unresolved in the particle spectra and constraining the total spin of the final states, rather than just the transferred angular momentum, by interpreting the γ-ray decay scheme. This makes the detection of γ rays a critical ingredient of direct reaction experiments and AGATA [1] excellent performance can enhance such studies significantly. The excellent energy and angular response is sufficient to perform lifetime measurements of states in the femtosecond range, using the Doppler shift Attenuation method (DSAM), as will be discussed in Sect. 4.2.

Low-energy Coulomb excitation (i.e. using beam energies of a few MeV per nucleon) is the only experimental method that can be used to determine spectroscopic quadrupole moments of short-lived excited nuclear states, which are directly related to their deformation. Moreover, it is unique in its sensitivity to relative phases of electromagnetic matrix elements involved in the excitation process. From extensive sets of $E2$ matrix elements, determined in Coulomb-excitation studies together with their relative signs, it is possible to deduce shape parameters (β_2, γ) of individual states using the quadrupole sum rules approach [2,3]. The sensitivity to both overall deformation of collective nuclear states, as well as their non-axiality, makes this experimental technique an ideal tool to study shape coexistence and shape evolution throughout the nuclear chart. Moreover, Coulomb-excitation cross sections to populate opposite-parity states can be related to $E3$ strengths, providing information on octupole collectivity.

Low-energy Coulomb-excitation studies employing AGATA benefit from its excellent Doppler-correction capabilities, as well as from a reduction in the peak-to-background ratio provided by the γ-ray tracking approach. This is particularly important for weak decay branches, observed on the Compton background of the dominating γ-ray transitions resulting from single-step excitation. Moreover, the greater granularity and efficiency with respect to previous-generation γ-ray spectrometers allow particle-γ-γ coincidences to be used for a clean separation of transitions forming doublets in singles γ-ray spectra. This will facilitate studies of nuclei that possess many γ-ray transitions in a narrow energy range, which is in particular the case of odd-A nuclei.

For intermediate-energy Coulomb-excitation measurements, which use beam energies of tens or hundreds MeV per nucleon, AGATA provides an even greater gain. Under such conditions, its unprecedented Doppler-correction capability and efficiency will make it possible to reach very exotic nuclei that currently are not accessible to γ-ray spectroscopy, leading to the identification of their lowest excited states and providing information about their collectivity.

2 The era before γ-ray tracking

Direct reaction studies have been performed so far by taking advantage from the first generation radioactive beam facilities and detection setups composed of Compton-shielded γ ray arrays, segmented silicon detectors and, where available, large acceptance magnetic spectrometers. Gamma-ray tracking was not available, but the work exploited segmented germanium arrays such as EXOGAM [4] at GANIL, MINIBALL [5] at CERN/ISOLDE and TIGRESS [6] at TRIUMF. The electrical segmentation provided position information for the γ-ray detection, which was vital to recover energy resolution when the velocity of the emitting nucleus approached $\sim 10\%$ of c.

2.1 TIARA-EXOGAM-VAMOS campaigns also including MUST2 at GANIL

The TIARA silicon array [7,8] was designed specifically to be operated with EXOGAM so that the power of high-precision γ-ray spectroscopy could be combined with charged-particle spectroscopy to study direct reactions with radioactive ion beams (RIB). In order to achieve sufficient efficiency, four EXOGAM detectors were arranged with their front faces as close as possible to the target (at 50 mm). The silicon geometry is thus extremely compact between angles of 35° and 145° and the energy spectra from the EXOGAM clover detectors (with four-fold segmentation within each of the four leaves of the clover) were subject to considerable Doppler broadening. This pioneering setup was installed in 2003 and was directed towards a study of ^{25}Ne via (d, p) [9] with a pure beam of ^{24}Ne from SPIRAL [10,11]. For such a reaction, the protons of interest emerge backwards of 90°. The results pointed to a rise in energy of the neutron $\nu d_{5/2}$ orbital and the emergence of N = 16 as a magic number as the Island of Inversion at ^{32}Mg was approached. At the limits of detection, certainly, but it was possible to analyse quadruple ^{25}Ne-p-γ-γ coincidences to confirm the γ-decay scheme and infer the spins of states [12]. The VAMOS magnetic spectrometer [13] was placed at zero degrees to record beam-like particles with full particle identification. The original TIARA setup was extended subsequently, with the addition of MUST2 telescopes [14] in the forward direction and this is shown in Fig. 1. This setup was able to discover the unbound intruder $\nu f_{7/2}$ state in ^{27}Ne, also using the (d, p) reaction. Further, however, the bound $\nu p_{3/2}$ intruder state at 765 keV was positively identified using a combination of both the γ-ray information and the proton angular distribution [15]. In

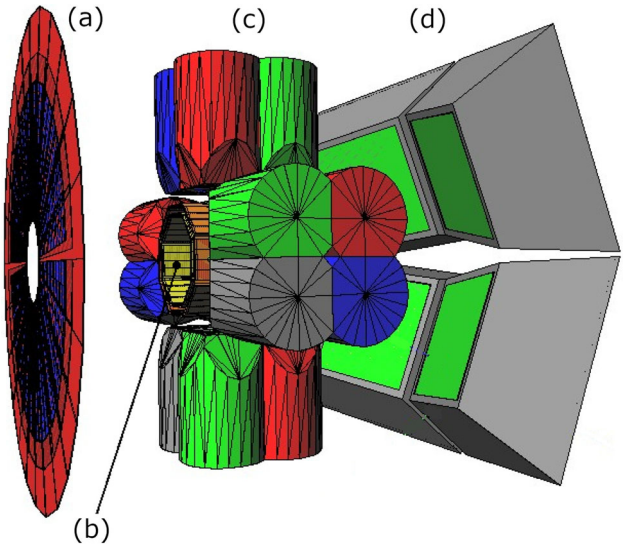

Fig. 1 The TIARA-MUST2-EXOGAM-VAMOS set-up at GANIL. From left to right, the SPIRAL beam enters via **a** the TIARA backwards annulus and **b** octagonal barrel - surrounded by **c** EXOGAM clovers - and followed by **d** the MUST2 forward telescopes. The clovers are placed at 90 degrees and 50 mm from the beam-spot on target for maximum detection efficiency. Beyond MUST2, particles entered the VAMOS magnetic spectrometer. Figure adapted from Ref. [18]

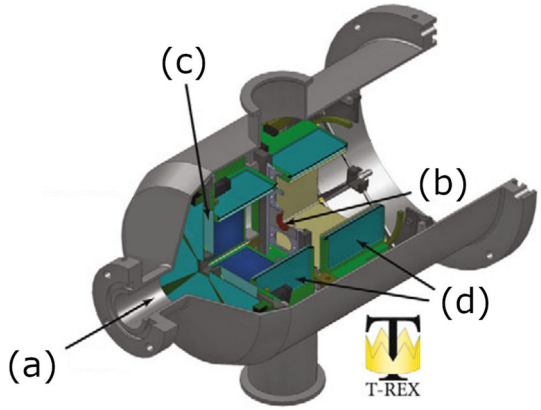

Fig. 2 The T-REX array is built to fit inside the compact germanium array MINIBALL at CERN/ISOLDE. At the left, **a** the beam enters the vacuum vessel to impinge at the target **b**, that is mounted in a ladder. At backward angles **c** an annular Si strip detector and one of two boxes of silicon detectors can record protons from reactions such as (d, p) and (t, p). In another box of Si detectors forward of 90° the elastically scattered target particles (e.g. d or t) can be detected. T-REX has generally operated without any detector at zero degrees for beam-like particles. Figure adapted from Ref. [20]

contrast, a previous study that was unable to detect the protons found that using just the γ rays did not give a definitive identification [16]. It is notable that the TIARA proton-γ results were obtained with a beam intensity from SPIRAL of just 2500 particles/s, indicating a bright future using a highly efficient array such as AGATA and the more intense beams from the newly emerging facilities. Another experiment with this setup employed a beam of ^{20}O from SPIRAL to study bound and unbound states in ^{21}O via (d, p) [17] and simultaneously ^{19}O via (d,t) [18,19]. In both cases, the γ rays were essential: in ^{21}O they showed that a particular unbound level selectively decays to the excited 2^+ state of ^{20}O, thus helping to pin down its spin, and in ^{19}O the population of the ground state and the 89 keV first excited state could be distinguished.

2.2 T-REX at CERN/ISOLDE

A compact array of silicon detectors, T-REX [20], was developed for use with reaccelerated beams from the ISOLDE facility at CERN. The array could be mounted inside the MINIBALL [5] segmented γ-ray spectrometer. The T-REX array (see Fig. 2) has quite restricted resolution in excitation energy because of the particular geometry of the strips but it has nevertheless produced some outstanding results that highlight the power of combining high-resolution γ-ray detection with charged particle detection in direct reactions. Using an innovative target of tritium loaded into a thin foil of titanium metal, the (t, p) transfer reaction adding two neutrons to ^{30}Mg was studied [21]. This led to the discovery of an excited 0^+ state at just 1058 keV excitation energy, consistent with a shape-coexistence scenario. The extensive array of radioactive species that can be accelerated at ISOLDE allowed the programme to extend upwards in mass towards closed-shell ^{68}Ni and ^{78}Ni isotopes.

The importance of γ-ray information for discerning between states that were unresolved in the particle spectrum was clearly demonstrated in a (d, p) study of ^{67}Ni [22] presenting particle energies versus γ-ray energies, similar to a spectrum from SHARC shown in Fig. 3). Another study employed the (d, p) reaction with a beam of ^{78}Zn to study ^{79}Zn and hence neutron orbitals near doubly magic ^{78}Ni [23]. Although the particle energy resolution was severely compromised, the data allowed the population on the second $d_{5/2}$ neutron orbital, which was tentatively identified. The arguments relied on high quality γ-ray data, again indicating that AGATA has much to offer for this kind of study.

2.3 SHARC at TRIUMF

Another of the particle arrays developed for transfer reaction studies is SHARC [24], which fits inside the TIGRESS array [6] of segmented clover Ge detectors at TRIUMF. A very challenging experiment, which depended intrinsically on having high-resolution γ-ray data together with the particle data, was mounted to study ^{26}Na, the isotone of ^{25}Ne studied earlier with TIARA. Since ^{26}Na is an odd-odd nucleus, the level scheme is rich with states, many of which are closely spaced in energy. The analysis [25] relied on using the γ-ray information to select individual states.

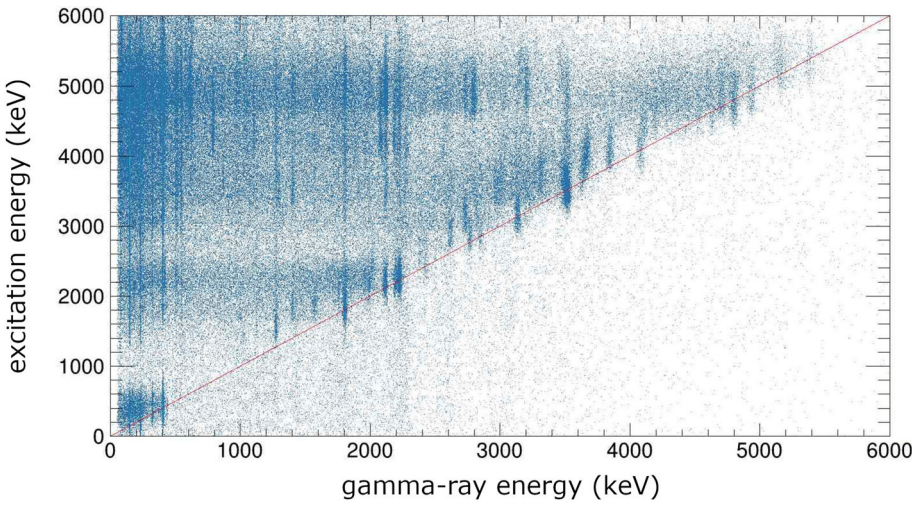

Fig. 3 Plot showing excitation energy in ^{26}Na (as determined from the energy and angle of protons from (d, p)) versus the much more highly resolved γ-ray energies from the decay of the corresponding states (as determined by Doppler correcting the measured energy). The experiment is described in Ref. [25]; this figure is adapted from one in Ref. [26] that reports further analysis of the same data

Another separate but equally important feature of the analysis was that the γ-ray energies enabled the excitation energies to be determined accurately. In fact, in the ^{26}Na study it was possible to extract angular distributions for protons by gating on appropriate γ-ray transitions. However, in experiments with poorer statistics the angular distributions required that ungated particle spectra were fitted for different angular bins. In such a case, it is vital to know the precise energy of every contributing state so that the fitting is properly constrained, and this requires γ-ray measurements.

2.4 The MUST2-TIARA-EXOGAM campaigns performed on LISE at GANIL

In spring 2009 a campaign of experiments was performed at GANIL focusing on the measurement of the (d, p) reaction induced by radioactive beams produced and separated by the LISE spectrometer. The shell-structure of neutron-rich nuclei around $N = 20$ and $N = 40$ were investigated using the ^{34}Si(d, p) at 19 MeV/u and ^{68}Ni(d, p) reactions at 28 MeV/u, respectively and the ^{60}Fe(d, p) at 27 A MeV was studied in order to provide a determination of the direct component of the ^{60}Fe(n,γ) radiative capture cross-section of astrophysical interest. For (d, p) measurements at the above energies, a good angular coverage of the backward hemisphere for the recoil protons is mandatory. Moreover, to cope with the absence of spectrometer for the detection of heavy residues, a good identification of the recoil protons is crucial. Therefore four MUST2 telescopes [14] were installed in the TIARA [7] vessel to cover the backward angles, see Fig. 4. The MUST2 telescopes were composed of the standard 300 μm-thick high granularity DSSD followed by a second layer consisting in the 5 mm thick Si(Li) detectors. The latter layer provided a residual energy measurement for particle identification and a sufficiently large increase of the dynamic range, at the expense of a 40% drop in geometrical efficiency due to the limited surface of the Si(Li) detectors. For the detection of γ rays in coincidence with the recoil protons, four segmented Ge EXOGAM [4] detectors were placed around the target in two different configurations. For the ^{60}Fe(d, p) measurement, the EXOGAM modules were placed at 5 cm from the beam axis. The target was shifted 4.2 cm upstream from the centre of these detectors in order to optimize the angular coverage of the MUST2 DSSD whilst keeping a γ-ray detection efficiency of 7% at 1 MeV. In the case of the ^{34}Si(d, p) and ^{60}Ni(d, p) reactions, the target was shifted 9 cm upstream from the center of the EXOGAM modules so as to avoid them shadowing part of the MUST2 detectors. The resulting γ efficiency was 3.8% at 1 MeV. Heavy residues emitted near zero degrees were detected in a 1.5 cm-thick plastic detector. In the case of the ^{34}Si(d, p) study, an ionisation chamber was placed upstream with respect to the plastic, so allowing for the selection of the Si residues. The results obtained for the ^{34}Si(d, p) reaction are reported in Ref. [27]. Energies and spectroscopic factors of states populated in ^{35}Si have evidenced a reduction by about 25% of the $\nu p_{3/2}$-$\nu p_{1/2}$ spin-orbit splitting, while the $\nu f_{7/2}$-$\nu f_{5/2}$ spin-orbit splitting seemed to remain constant. These features were attributed to the properties of the two-body spin-orbit interaction. Concerning the ^{68}Ni(d, p), a strong population of the $9/2^+$ ground-state was observed and the extracted spectroscopic factor was found to be in agreement with shell-model calculations. At higher excitation energies, a broad bump centered at around 2.5 MeV and containing a sizeable amount of $\ell = 2$ state, attributed to the population of the $d_{5/2}$ orbital has been observed [28]. However, the poor energy resolution due to the target thickness together with the weak sensitivity of angular distributions on the transferred-ℓ did not allow the components involved to be disentangled. A new measurement will be performed at GANIL/LISE in the near future with the MUGAST-EXOGAM setup. Finally, from the ^{60}Fe(d, p) study, the direct capture component con-

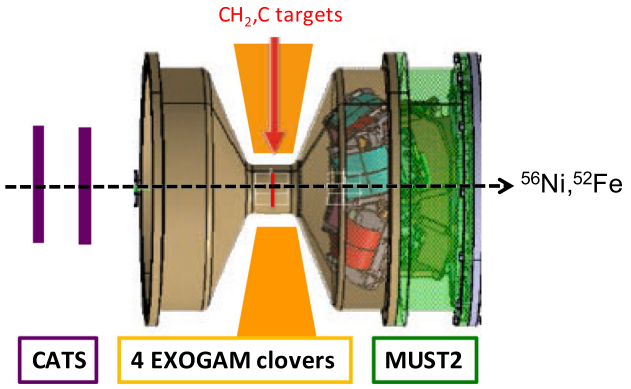

Fig. 4 The TIARA-MUST2-EXOGAM set-up at GANIL. From left to right, the CATS beam tracking detectors, the TIARA backwards end-cap and barrel followed by the MUST2 forward telescopes. EXOGAM clovers are placed at 90 degrees close to the target position to enhance the detection efficiency

tribution to the ^{60}Fe(n, γ) capture reaction, thought to be the main process for the destruction of ^{60}Fe inside massive stars during convective He and C shell burning, was estimated to be negligible, pointing to the dominance of the resonant capture [29].

The LISE campaign of 2014 employed a set-up, see Fig. 4, evolved from that used in 2009. The beam was tracked to the target by two CATS [30] devices. A set of 4 MUST2 telescopes in the forward direction were combined with TIARA in the backward direction and the TIARA barrel around 90 degrees for particle detection. The MUST2 detectors placed at 18 cm from the target were covering from 8 to 40 degrees whereas the ball was covering the most backward angles from 144 to 169 degrees. Four EXOGAM clovers were surrounding the target at 90 degrees at a distance of 5.5 cm. The configuration gives a photopeak efficiency at 1.3 MeV of 8%. This large efficiency is obtained at the expense of the angular resolution. Indeed with a beam velocity of $\beta = 0.25$, the Doppler broadening is $\Delta E/E_0$ is 0.09.

This campaign addressed two different physics cases: the search for neutron-proton (np) pairing through two-nucleon transfer in the *fp*-shell [31] and the investigation of the low-lying states in ^{17}C in the context of the $N = 14$ shell closure [32]. Both required the combination of particle and γ-ray measurements in coincidence to unambiguously assess the states populated in the transfer reaction.

Neutron-proton pairing is a unique feature of the nucleus where two different fermion fluids can form pairs of neutron-proton. These pairs can occur either in the isovector (T = 1) or isoscalar (T = 0) channel. This phenomenon manifest itself mostly in the $N = Z$ nuclei due to the large overlap between the neutron and the proton wavefunctions. High-j orbitals are also more favourable as the typical number of pairs entering into play depends on the degeneracy of the specific orbitals involved. The signature of the departure from the single particle structure and the onset of superfluid phase is given by the increase of the cross-section for two-nucleon transfer between the ground states of nuclei A and A±2 with a maximum reached at mid-shell. In the case of np pairing, starting from an even-even A nucleus ($J = 0^+$,T = 0), two states can be populated ($J = 0^+$,T = 1) and ($J = 1^+$,T = 1). The ratio of the cross-sections $\sigma(0^+)/\sigma(1^+)$ reflects the relative strength of the isoscalar and isovector channels. The goal of the experiment was to measure two-nucleon transfer (p,^{3}He) on an open shell nucleus, ^{52}Fe and a doubly magic nucleus ^{56}Ni to give the trend of the ratio over the *f*-shell. As the residual nuclei are odd-odd nuclei, the high density of states requires the combination of particle and γ-ray detection in order to identify the populated states. Due to the very low cross-section (few tens of microbarns), thick targets (7 mg/cm^2 CH_2 targets) were used which leads to an excitation energy resolution of about 1.4 MeV. Given that the low lying level scheme of the residual nuclei is known, the γ-ray spectra obtained by gating on the region of interest of the excitation energy allowed to determine the cross-section for each state and to remove the contribution from the top-feeding levels. The angular distribution was only extracted for the ground state due to the lack of statistics for the first excited state and were well-reproduced by second-order DWBA calculations using two-nucleon amplitudes provided by shell model calculations using the GXPF1 interaction. The cross-sections determined experimentally were compared with the same calculations. No evidence for an isoscalar deuteron-like (J = 1,T = 0) pairing condensate was found.

The study of the evolution of the shell model in the light neutron-rich nuclei has shown the emergence of $N = 14$ and $N = 16$ a sub-shell closures, with ^{22}O and ^{24}O being doubly-magic nuclei. However, the $N = 14$ gap does not persist at $Z = 6$ in the carbon chain [33]. This may be explained in terms of proton-neutron interactions and the absence of $p_{1/2}$ protons in carbon. Shell model calculations based on phenomenological two-body interactions have struggled to reproduce the structure of both the neutron-rich C and O isotopes. The investigation of the low-lying single particle states of ^{17}C through the one-nucleon transfer reaction ^{16}C(d, p) provides further detailed spectroscopic information to test the shell-model interactions. As the energy resolution of TIARA could not resolve the three states of interest, the coincident γ-ray measurement was used to select the protons from transfer to each populated state. It was found that the $3/2^+$ ground state has a very small spectroscopic factor so that the $\nu d_{3/2}$ strength is carried by unbound states. In contrast, the two first excited states exhaust a large fraction of the available single-particle strength expected for a pure $(\nu 1d_{5/2})_2$ neutron configuration in ^{16}C ground state: ≈ 70 % for the $(\nu 1d_{5/2})$orbital and ≈ 100 % for the $(\nu 2s_{1/2})$ orbital. The size of the $N = 14$ gap can be estimated from the exci-

tation energies of the two first excited states and gives −0.12 MeV, indicating the absence of an $N = 14$ gap.

3 Advances with AGATA

The advent of γ-ray tracking technology assisted by the development in large-area uniform and highly segmented silicon detectors and the presently ubiquitous digital electronics has produced great advances in sensitivity and, therefore, in the range of physics accessible. In the following, the use of current detection systems aiming at cutting-edge measurements will be presented as a showcase of the unprecedented performances of modern set-ups.

3.1 The AGATA-MUGAST-VAMOS campaign at GANIL

The MUGAST-AGATA-VAMOS set-up (Fig. 5) combines the MUGAST Silicon array [34] with AGATA array [35] and the large acceptance VAMOS spectrometer. It offers the unique opportunity to perform exclusive measurements with the radioactive beams produced by the SPIRAL1 facility at GANIL and to use solid or cryogenic targets like the HeCTOr ^{3}He target [36]. Five experiments were performed during the campaign addressing physics cases related to the study of unbound nuclei and their one- and two-proton decay, nuclear astrophysics and reactions relevant for type I X-ray bursts, proton and neutron spectroscopy at $N = 28$ and lifetime measurement of states populated by transfer. Neutron, proton and alpha transfer were investigated as well as resonant elastic scattering with beam intensities from 10^4 pps up to 10^8 pps showing that the system is very versatile.

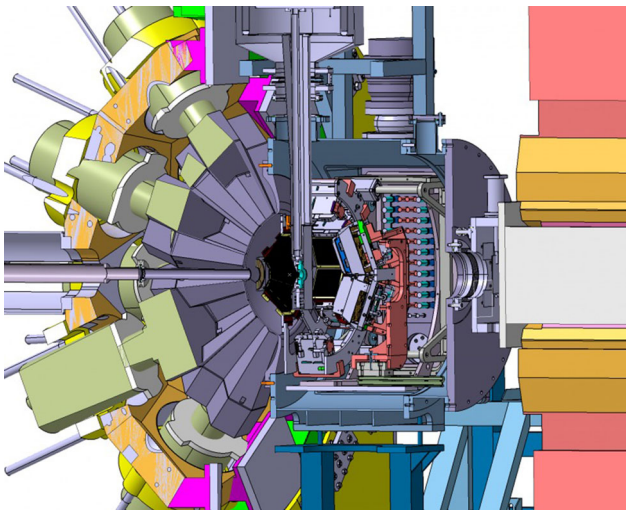

Fig. 5 The MUGAST-AGATA-VAMOS set-up at GANIL. From left to right it is possible to see the AGATA array covering the backward hemisphere with respect to the bean direction, from left to right in the figure. In the centre, the reaction chamber hosting the MUGAST array and compatible with the cryogenic target on the upper part, is visible. Finally, on the right-most part the entrance of the VAMOS magnetic spectrometer starts to be seen

The MUGAST array comprises 4 MUST2 telescopes in the forward direction coupled with up to 7 trapezoidal 500 μm thick DSSDs in the backward hemisphere and an annular detector for the most backward angles and a square 300 μm thick DSSD at 90 degrees. It covers from 8 to 50 degrees in the forward direction and from 100 to 170 degrees in the backward angles with a geometrical efficiency of 70% in average.

A major challenge in the coupling of silicon arrays to γ-ray arrays is the transparency. The photopeak efficiency at 1.4 MeV was measured to be 4.9(1)% with 41 fully operational crystals placed at 182 mm from the source and 7.1(1)%after neighbouring crystal add-back procedure was applied. Moreover, the comparison with the plunger device chamber shows that the MUGAST chamber and detectors do not induce additional absorption for γ-ray energies above 200 keV and are ∼10% more transparent than a plunger set-up at 100 keV.

The VAMOS magnetic spectrometer provides full identification of the heavy residues from the reaction as well as full rejection of parasitic reactions such as fusion-evaporation when combined with MUGAST identification of light particles. With the configuration used during the campaign, the efficiency in the determination of the magnetic rigidity is 90%, taking into account the drift chamber detection and the reconstruction method efficiencies (time-of-flight or energy loss versus total energy or mass, charge and total energy). The detection efficiency of the ionisation chamber is better than 92% for each section of the detector.

The triple coincidence measurement is an asset as it provides full characterisation of the nucleus of interest through its γ decay but also its particle decay, the entry point for the γ decay through particle measurement, excellent background rejection, precise monitoring of the target thickness and Doppler correction from the two-body kinematics of the reaction.

In AGATA, the Doppler correction of in-flight emitted γ ray is usually performed event-by-event using the first hit interaction position with the positions and energies given by the pulse shape analysis algorithms, and the averaged β of the beam. In the case of the measurement of ^{19}O(d, p) reaction, a resolution (FWHM) of ∼10 keV is obtained for the 1.673 MeV γ-ray transition from the de-excitation of the 2^+_1 state in ^{20}O using an average beam velocity of 12.6%. The VAMOS spectrometer could only be used as a ToF separator due to the high intensity of the impinging beam. However, the combination with MUGAST brings in this case an alternative and powerful method for Doppler correction based on the two-body kinematics by using the momentum of the heavy-ions deduced from the precise position and energy measure-

ment of the light charged particle. Given the high granularity of MUGAST, this method improves the resolution and gives in the same conditions 7.1 keV.

The major challenge with high intensity beams (up to 10^8 pps) is the particle identification by time-of-flight. Beam tracking devices cannot be used and the time-of-flight relies on the RF from the beam with a resulting resolution of ∼2.5 ns for SPIRAL1 beams. Therefore, the timing between MUGAST and VAMOS was investigated for the first time, by reconstructing the trajectories of heavy-ions in VAMOS. The final time-of-flight resolution was 1.4 ns, mainly due to the 1 ns jitter of the MUGAST signals, that farther extends the particle identification to higher energies.

3.2 Transfer reaction spectroscopy

3.2.1 Search for γ rays from the unbound ^{15}F nucleus

The nucleus ^{15}F is unbound and is located two neutrons away from the proton drip-line. Contrary to naive expectations, the widths of the ^{15}F excited states do not broaden with higher excitation energy. In particular the negative parity states of ^{15}F are at least one order of magnitude narrower than the ground state ($\Gamma_{1/2+} \sim 500$ keV). This could be a consequence of the proximity of these states to the nearby 1, 2 and 3 proton decay thresholds [37–39].

The observation of radiative transitions between unbound states is a rare phenomenon that has only been observed in very few experiments [40,41]. Due to their longer lifetimes, narrow states should be the perfect experimental candidates to observe such γ-ray transitions. As a consequence, the second excited state of ^{15}F, the $1/2^-$ state, with a width of 36 keV, seems to be an ideal case.

The presence at GANIL of the state-of-the-art experimental setup composed of MUGAST, VAMOS and AGATA made possible the invariant mass measurement of ^{15}F excited states. The two proton decay of the $5/2^-$ and $3/2^-$ states were measured from the triple coincidence of two protons in MUGAST and ^{13}N in VAMOS [39]. The decay of $1/2^-$ state in ^{15}F was populated with the ^{1}H(^{14}O, $p\gamma$)^{14}O reaction using the triple coincidence of one proton in MUGAST, ^{14}O in VAMOS and γ-ray in AGATA. Presently, no γ ray, consistent with the expected $E_r \sim 3500$ keV $\pm$ 500 keV state, was observed. Considering the detection efficiency of MUGAST, VAMOS and AGATA and taking into account the beam intensity (monitored during the experiment) and the target thickness (92.3(9) μm) a preliminary upper limit for the width and branching ratio can be obtained $\Gamma_\gamma < 4.4(1.5)$ eV and $BR_\gamma < 0.02(1)$ %.

3.2.2 Spectroscopy of bound states produced in transfer

The MUGAST setup with AGATA and VAMOS is ideally suited to transfer reaction studies in general, and two of the measurements performed serve to highlight the immense benefit of AGATA's excellent Doppler correction (and hence energy resolution):

– ^{47}K(d, p)^{48}K for nuclear structure, and
– ^{15}O(^{7}Li, t)^{19}Ne for nuclear astrophysics,

both of course in inverse kinematics.

The study of ^{48}K takes advantage of the unique situation in the neutron-rich potassium isotopes where the odd proton is surprisingly found in the $\pi s_{1/2}$ orbital, with the $\pi d_{3/2}$ orbital filled (this is known from magnetic moment measurements [42]). The transferred neutron in the (d, p) reaction populates empty orbitals in the fp-shell above the $\nu f_{7/2}$ orbit, providing a rare opportunity to probe the interactions between protons and neutrons in such disparate orbitals. This information will be vital when experiments can study the lighter isotones in detail. The results, still preliminary, show how the excellent γ-ray energy resolution allows the relatively complicated spectrum of odd-odd ^{48}K to be untangled [43]. An example is shown in Fig. 6.

The study of ^{19}Ne addresses a famous and important problem in nuclear astrophysics. The capture reaction (α, γ) on ^{15}O to make ^{19}Ne forms a bottleneck at the start of the rp-process that drives X-ray bursts, when hydrogen-rich material encounters the surface of a neutron star. The production of heavy elements depends on the rate of the alpha capture reaction by ^{15}O compared with its rate of beta-decay. The alpha capture rate in turn depends upon the partial width for alpha decay, Γ_α, of any resonant states just above threshold, at energies reached by alpha-particles in the hot environment. The state in ^{19}Ne at 4.03 MeV has long been known to be the dominant contributor to the rate but the crucial value of Γ_α has eluded accurate measurement. This is because the 4.03 MeV state almost always decay by γ-ray emission and the alpha-particle decay is a vanishingly small component of the total decay. In the present experiment [44] the idea is that (a) the 4.03 MeV state is populated in a reaction that has a cross section that directly measures Γ_α and (b) if the state is populated then it will decay by γ-ray emission. Hence, the number of γ rays observed at 4.03 MeV is a direct measure of Γ_α, as long as the reaction mechanism is reliably understood. The reaction employed was (^{7}Li, t) to transfer an alpha-particle cluster on to ^{15}O.

The energy spectrum of γ rays recorded using AGATA is shown in Fig. 7 and represents preliminary results from Ref. [45]. The region where the 4.03 MeV γ-ray peak would fall is expanded. The spectrum is extremely low in background due to the triple coincidence requirement: the experiment

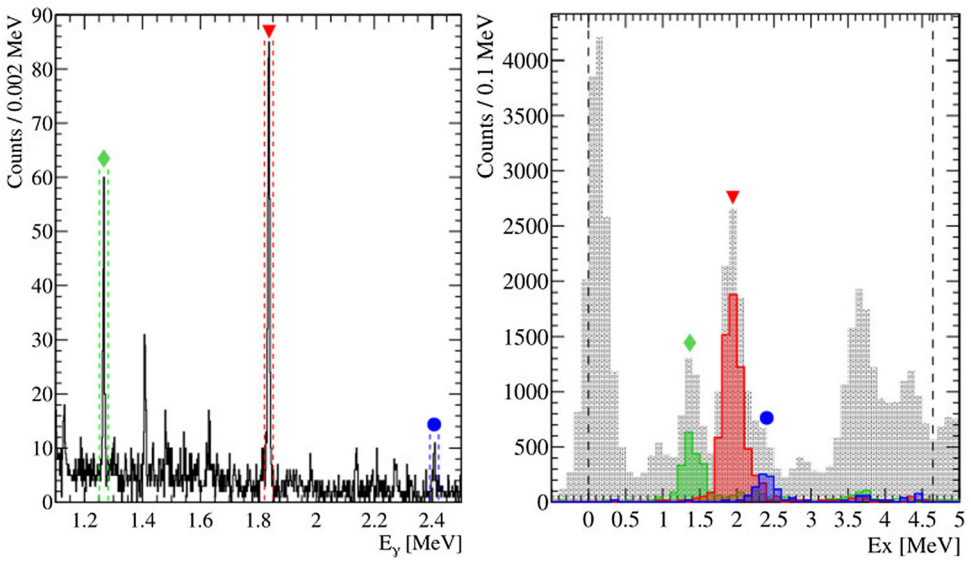

Fig. 6 In the left panel, a zoomed region of the γ-ray energy spectrum is shown and on the right there is an excitation energy spectrum derived from the measured protons. The γ rays were in coincidence with a particle in the MUGAST array and a particle reaching the focal plane of VAMOS. Three peaks are highlighted by a ♦, a ▼ and a •. In the right hand panel, the computed excitation energy spectrum is shown in the background in a light colour, corresponding to the data from all protons in MUGAST in coincidence with VAMOS. The coded symbols show the individual contributions made by states that decay via the indicated γ-ray transitions. Overlapping states in the particle spectrum are thus clearly isolated. In fact, the small γ-ray peak near 2 MeV corresponds to the decay of a state that falls between the ▼ and the • states. [C. Paxman, University of Surrey, private communication]

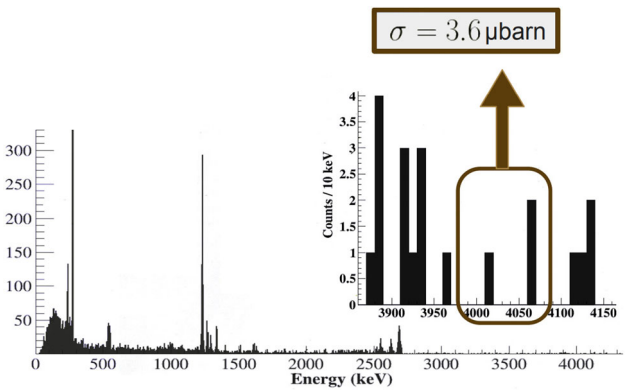

Fig. 7 Preliminary γ-ray energy spectrum from the reaction ^{7}Li(^{15}O, t γ)^{19}Ne [45]. The analysis selected ^{19}Ne-t-γ triple coincidences. The value for the cross section, after being confirmed and interpreted using reaction theory, will yield a value for the partial width for alpha-decay, Γ_α, of the 4.03 MeV state. This partial width is critical in determining break-out from the hot-CNO cycle on the surface of neutron stars, and therefore the probability of thermal runaway towards an X-ray burster

detected the triton in MUGAST, the ^{19}Ne in VAMOS and the γ rays in AGATA. The three counts in the region of interest, if taken at face value, would correspond to the extremely small cross section of 3.6 μb for the 4.03 MeV state. Further analysis will be required in order to refine this preliminary value and to provide an estimate of the uncertainty.

The two spectroscopic transfer studies above were both performed with reaccelerated radioactive (ISOL) beams. It is of interest also to know how a γ-ray tracking array such as AGATA can improve these studies using fragmentation beams. A transfer experiment has however been performed using the γ-ray tracking array GRETINA [46] which in the USA is present implementation of the complete 4π GRETA array which is under construction. The experiment itself [47] was again astrophysically motivated and ingeniously used the (d, p) neutron transfer reaction on the 0^+ ground state of ^{26}Si in order to study proton capture onto the isomeric excited 0^+ state of ^{26}Al, the isobaric analogue of the ^{26}Si ground state: a mirror reaction on a mirror nucleus to reach the identical final state in ^{27}Si. The γ-emitting nuclei were moving at 0.25c and the γ rays of interest extended up to energies above 6 MeV. Two factors limited the precision of the angular determination for γ rays: firstly, the localisation of the γ-ray interaction via tracking techniques was not yet fully implemented and secondly the beam spot on target was extended due to the use of dispersion-matched focusing into the magnetic spectrometer mounted beyond the target. The energy resolution of the Doppler-corrected peaks as shown in Fig. 8 is nevertheless impressive.

3.2.3 Transfer reactions with ^{3}He cryogenic target

Direct reactions offer a unique insight into the nuclear structure and the underlying shell effects in a nucleus. The combination of the AGATA spectrometer with segmented silicon detectors, a magnetic spectrometer, and a cryogenic target opens the possibility of in-depth studies of isotopes faraway from the valley of β stability.

In particular, the ^{46}Ar(^{3}He, d)^{47}K direct reaction was exploited to infer relative spectroscopic factors for the proton-transfer to the low-lying single-particle (SP) states of ^{47}K. In the shell-model picture, spectroscopic factors of SP states represent a direct link with the concept of shell

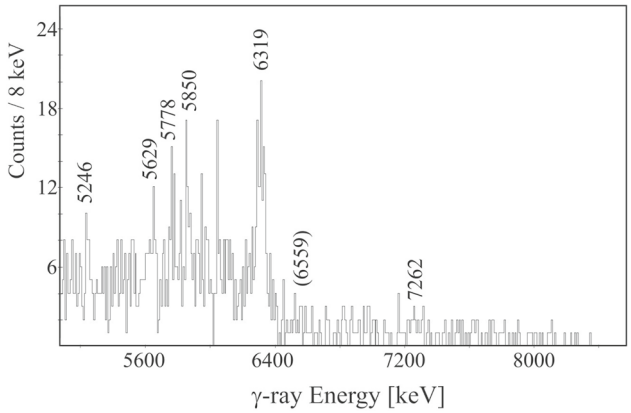

Fig. 8 Gamma-ray energy spectrum from reaction products moving at $0.25c$ through the GRETINA γ-ray tracking array [46]. The transitions are from excited states in ^{27}Si. The reaction was (d, p) transfer induced by a beam of ^{26}Si made by projectile fragmentation at the NSCL facility, MSU. The energy resolution FWHM obtained in the 6.5−7.0 MeV region was $\simeq 0.7\%$ (see text). Figure adapted from Ref. [47]

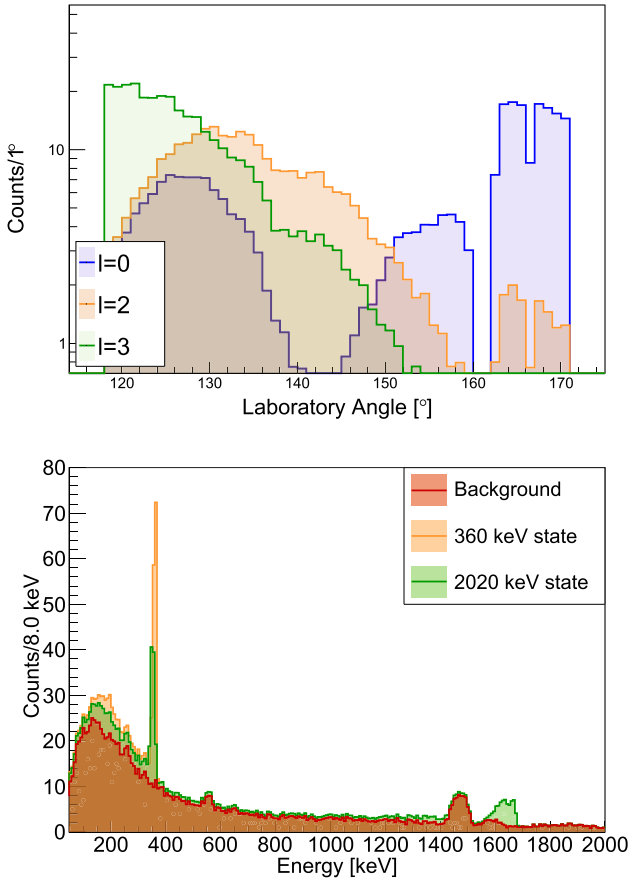

Fig. 9 (Top panel) Monte-Carlo simulation of the experimental response of the setup for the three different transfer channels performed with Geant4 and based on finite-range DWBA calculations. (Bottom panel) Monte Carlo Geant4 simulation of the response of AGATA to the population of the $3/2^+$ and $7/2^-$ states of ^{47}K

occupancy. In the case of interest, the experiment focused on extracting the probability of populating the $1/2^+$ (g.s.) and $3/2^+$ (360 keV of excitation energy) of ^{47}K to obtain information on the proton contribution in the ground state of ^{46}Ar. Additionally, the direct population of the $7/2^-$ second excited state (2020 keV) was observed. From the nuclear structure point of view, ^{46}Ar has been a hot topic due to the discrepancy between shell-model calculations and lifetime measurements of the quadrupole transition probability (B(E2)) between the g.s. (0^+) and the first excited state (2^+) [48]. The overestimation of this quantity by the shell model with the SDPF-U interaction has been linked to the proton component of the wave function [49].

The radioactive ^{46}Ar isotopes were produced from the fragmentation of a primary ^{48}Ca beam impinging on a graphite target. The extracted isotopes were post-accelerated at an energy of 9.9 MeV/u and delivered to the experimental hall with an average intensity of 4×10^4 pps. The experimental setup consisted of VAMOS, AGATA, MUGAST, the beam tracker CATS2 and a gaseous ^{3}He cryogenic target HECTOR. This last is composed of a 3-mm thick cell with 3.8 μm HAVAR containment windows cooled to 7 K to achieve an effective density, suitable for low-intensity radioactive beams, of $\approx 1.5 \times 10^{-3}$ g/cm^2, equivalent to $\approx 5.0 \times 10^{-3}$ g/cm^3.

The setup allowed for the detection and identification of both the heavy fragment, in VAMOS, and the deuteron, in MUGAST. The angular distribution, compared by means of a likelihood maximization, allowed the extraction of the probability of populating the g.s. ($\ell = 0$) and the $3/2^+$ state ($\ell = 2$). Figure 9 shows the sensitivity of the setup to two different types of transfer.

At the same time, the possibility of detecting γ rays emitted by the excited levels of ^{47}K offers some virtually independent verification of the experimental outcome. The full potential of the AGATA tracking spectrometer was exploited as the long-lived populated states ($T_{1/2}(3/2^+) = 1.1(3)$ ns and ($T_{1/2}(7/2^-) = 6.3(4)$ ns) decayed on average beyond the target position and towards the entrance of the magnetic spectrometer. The response of the spectrometer is sensitive to the different lifetimes and can be precisely estimated with Monte Carlo Geant4 simulations, at odds with conventional collimated Compton-shielded HPGe detectors, that would not be able to detect γ rays from such a long-lived state.

Triple γ-d-^{47}K coincidences between AGATA, MUGAST, and VAMOS showed the emission of a few 360 keV γ rays. The emission can be related to a direct population of the state ($\ell = 2$ transfer) or to the feeding from the $7/2^-$ state ($\ell = 3$). The combination of the high resolution of AGATA with the event-by-event Doppler correction provided by VAMOS allowed for a narrow gate in correspondence of 360 keV

which revealed the excitation energy linked to the emission of these photons and thus the populated level.

Additionally, the AGATA-VAMOS coincidence was exploited as an independent assessment of the probability of populating via $\ell = 2$ of $\ell = 3$ transfer. Figure 9 (bottom panel) shows the effect on the response caused by the difference in efficiency owing to the different lifetimes. The Doppler broadening of the 1660 keV γ ray is caused by the uncertainty on the position of decay of the isotope.

3.3 Nuclear lifetime measurements via transfer

Direct transfer reactions, where one, two nucleons or a cluster are exchanged between projectile and target, are promising tools for the measurement of the lifetime of nuclear excited states. The lifetime of most low-lying nuclear excited states lies in the range between few fs (10^{-15} s) and few ns (10^{-9} s) and can be measured with techniques that rely on the Doppler shift of the energy a γ ray when it is emitted by a nucleus in flight. Such measurements are affected by systematic errors when possible slow feeding transitions on the state of interest cannot be properly controlled. In this case, the lifetime of the state is overestimated and, as a consequence, the associated transition probability underestimated.

If a particle detector is in coincidence with the γ-ray spectrometer, one can in some cases reconstruct the excitation energy of the nucleus of interest and suppress the contribution of feeding transitions with appropriate gates. This is normally the case for binary reaction as transfer ones. In multi-nucleon transfer reactions with heavy ions, usually the identification of one of the reaction products is obtained by means of a magnetic spectrometer, like VAMOS at GANIL or PRISMA at LNL. In this case the control on possible feeding transitions is made difficult by the resolution in Total Kinetic Energy Loss (TKEL), which is of the order of few MeV, and the fact that in these reactions both reaction partners are excited, so the measured TKEL distribution represents the contribution of both excitation energies. In direct transfer reactions the detection of the light ejectiles in a detector (usually a Silicon array) in coincidence with the γ-ray array allows to reconstruct the excitation energy of the heavy recoil with resolutions ranging from tens to hundreds of keV, depending on the specific case. In addition direct reactions provide greater selectivity and higher cross sections for a specific set of excited states.

With the improvement of the performances of γ-ray and particle detection arrays in terms of efficiency, selectivity and resolution, the experimental investigation of nuclei far from the stability has moved to more exotic isotopes and to the study of nuclear properties that are less accessible. In fact, until recent years experiments involving direct reactions using RIB were restricted to nuclear spectroscopy, but now they are being extended to lifetime measurements using techniques such as the Recoil Distance Doppler-Shift (RDDS) method [50] and the Doppler Shift Attenuation Method (DSAM) [51].

3.3.1 *Lifetimes in ^{20}O*

With the new generation of γ-ray arrays and the leap in sensitivity, experimental nuclear physics has reached a level of precision that allows the comparison with state-of-the-art *ab-initio* calculations also for rare exotic systems.

In this context, the oxygen isotopic chain represents an ideal region for the comparison. This region has attract interest in the past around the anomaly of the neutron dripline. In fact, if standard shell-model calculations predict the ^{28}O ($Z = 8, N = 20$) to be the last bound isotope, it was observed experimentally that ^{24}O is the heaviest bound oxygen isotope. This anomaly was explained by Otsuka and collaborators [52] by adding the contribution of three-body forces in the calculations, that have the effect of changing the single-particle energies of the *sd* orbitals and correctly reproducing the observed dripline. In recent years, *ab-initio* calculations have started including three-body terms: the ^{20}O nucleus represents a textbook case. In fact, this isotope, being only two neutrons apart from the last stable isotope, is easily accessible experimentally. The non-yrast states, 2_2^+ and 3_1^+, are based on a mixed configurations of $(d_{5/2})^3(s_{1/2})^1$ orbitals and their properties such as the excitation energy and the reduced transition probabilities are expected to be influenced by the three-body forces.

The ^{20}O nucleus was populated in a direct reaction where a single neutron was transferred from the target to the beam isotope. The radioactive ion beam of ^{19}O was provided by the SPIRAL1 complex in GANIL and post-accelerated to an energy of 8 *A*MeV, with an average intensity of 4×10^5 pps and a purity above 99%. The beam impinged on a deuterated polyethylene target (CD_2). Two types of target were employed: a self-supporting 0.3 mg/cm^2-thick CD_2 target, for spectroscopy measurements, and a CD_2 target of the same thickness deposited on a 24.4 mg/cm^2-thick degrader of ^{197}Au, employed to perform lifetime measurements using the DSAM.

The beam-like recoils were emitted at forward angles and detected using the VAMOS spectrometer, while protons emitted at backward angles were detected using the MUGAST array. The time-of-flight measurements between VAMOS, MUGAST and the radiofrequency of the cyclotron were employed to separate the events of interest, namely the transfer reaction events, from the parasitic reactions such as fusion-evaporation and fusion-fission on the carbon and gold nuclei of the target and degrader. From energy and angular information of the proton detected with MUGAST, it was possible to reconstruct the kinematics of the beam-like part-

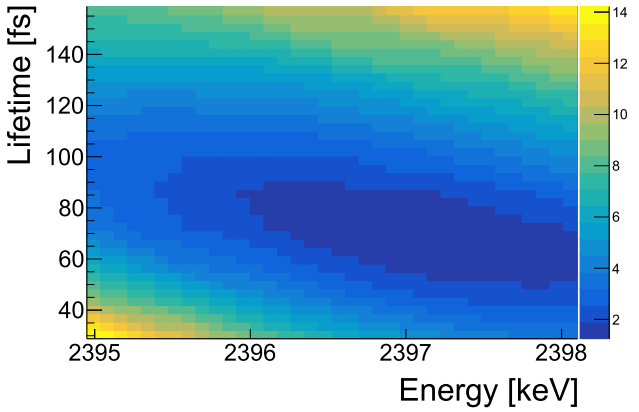

Fig. 10 χ^2 surface as a function of the lifetime of the 2_2^+ state and energy of the $2_2^+ \rightarrow 2_1^+$ transition. The minimum is found for a lifetime between 60 and 70 fs

ner: in particular, the energy, the velocity vector and the excitation energy.

Finally, the γ rays emitted by the ^{20}O nucleus were detected by the AGATA array, placed at backward angles with respect to the beam direction. By combining the information on the velocity vector of the beam-like partner and the position of first interaction of the γ ray in AGATA, it was possible to perform a Doppler correction on a even-by-event base, using the velocity at the reaction point.

The combination of the high selectivity of VAMOS and MUGAST and the good Doppler correction energy reconstruction led to extremely clean spectra with a high peak-to-total ratio that allowed the identification of weak γ-ray transitions that were never observed before. By applying selective gates on the excited states reconstructed with MUGAST, it was possible to perform γ-particle spectroscopy and reconstruct the level scheme of the nucleus.

The dataset collected using the self-supporting CD_2 target was employed not only for the spectroscopic study of the nucleus, but also to validate the kinematic reconstruction of the heavy partner and optimize the realistic parameters for the Monte Carlo simulation, such as the intrinsic resolution of the germanium detector, the smearing of the particle and γ rays and the measured angular distributions of the excited states [53,54].

Then a series of realistic simulations have been performed by varying the lifetime of the states of interest and the energy of the transitions in a sensible range. The normalised simulations were then compared with the experimental spectra using the least-χ^2 method to identify the minimum and extract the lifetime of the states, as shown in Fig. 10. The statistical errors were determined by using the $\Delta\chi^2 = 1$ constraint. A similar approach has been used in Refs. [55,56].

In order to eliminate the influence of the observed and unobserved feeders, a gate on the excitation energy of the ^{20}O has been applied in order to select only the events coming from the direct population of the state of interest. The importance of this gate, that is possible thanks to the use of direct reaction, is proved by the fact that by applying the same analysis method without the gate, the lifetime of the 2_2^+ state results to be 30% longer, introducing a systematic error.

3.3.2 Lifetimes: preparation for SPES@LNL

The AGATA spectrometer was in 2021 reinstalled at LNL [57], where it was for the first time operational and successfully run for a 2-year-long campaign during 2010-2011 [58] with a variety of auxiliary detectors [59]. Recently, the full AGATA performance was exploited at LNL to measure the lifetime of intruder states in the nucleus ^{37}S ($Z = 16$, $N = 21$), at the upper border of the $N = 20$ Island of Inversion [60]. In this nucleus, at variance with its isotone ^{39}Ar with $Z = 18$, significant γ-decay branchings between the so-called *intruder* states, built on $2p - 1h$ or $3p - 2h$ excitations above the $N = 20$ shell gap, and *normal* states were observed. In particular, the $3p - 2h$ $7/2_2^-$ intruder level at 2023 keV has a strong E2 decay, with a branching ratio of about 35 %, to the spherical $1p$ $3/2_1^-$ level at 646 keV which is not reproduced by state-of-the-art Shell Model calculations. This may represent a sudden increase in the collectivity of the intruder configuration, or a mixing of the spherical $3/2_1^-$ state with intruder configurations. The determination of reduced transition probabilities can shed light on the nature of such excitations and help characterise the beginning of the development of the Island of Inversion.

Intruder states in ^{37}S were populated via the direct transfer reaction d(^{36}S, ^{37}S)p. The ^{36}S beam, delivered by the TANDEM accelerator at an energy of 164 MeV ($\sim$4.5 MeV/u) and average intensity of 0.1 pnA, impinged on a 500-μg/cm^2 thick CD_2 target. The ejected protons were detected in the SPIDER detector [61] placed at backward angles and covering an angular range in θ_{lab} from 124° to 161°. SPIDER consists of seven trapezoidal Si detectors segmented into eight annular strips and arranged in a conical geometry, The γ rays coming from the de-excitation of ^{37}S were detected in coincidence in the AGATA spectrometer.

The expected lifetimes of the states of interest lie in very different ranges, tens or hundreds of ps for the $2p - 1h$ $3/2^+$ intruder state and hundreds of fs for the $3p - 2h$ $7/2_2^-$ state. In this experiment both lifetimes could be measured simultaneously by combining the DSAM and RDDS methods. The CD_2 layer was evaporated on a Au backing of $\sim$5 mg/cm^2 and installed on the Plunger device, which allowed to vary in a controlled way the distance between the CD_2+Au target and a Ta stopper of 30 mg/cm^2. The slowing down of the ^{37}S ejectile in the Au backing allows to measure the shorter lifetime of the $7/2_2^-$ state with the DSAM technique. The ion then de-excites travelling the distance between the target and the stopper. By computing the ratio between the num-

ber of γ rays emitted in flight and stopped as a function of the target-to-stopper distance, one can determine the long lifetime (~ 100 ps) of the $3/2^+$ state.

The top panel of Fig. 11 shows, as an example, a preliminary experimental γ-ray energy spectrum obtained by requiring a coincidence with SPIDER. The γ-ray energy of the $3/2^-_1 \rightarrow 7/2^-_{gs}$ transition at 646 keV, Doppler-corrected on an event-by-event basis considering the energy of the proton measured in SPIDER, is plotted versus the angle between the γ ray and the ^{37}S ejectile. The in-flight component, associated to γ rays emitted before the ion has reached the stopper, appears here at the correct energy and is well separated from the stopped component, associated to γ rays emitted after the ion has reached the stopper. The continuous angular distribution, made possible by the tracking capabilities of AGATA, gives also the possibility to perform a 2D analysis to determine the lifetime [62].

The bottom panel of Fig. 11 shows two simulated γ-ray energy spectra for the $7/2^-_2 \rightarrow 7/2^-_{gs}$ for different assumed lifetimes of the level. Given the short lifetime predicted for this level, it is important to control possible feeding transitions coming from higher-lying level. This is done by detecting the recoil protons in SPIDER and reconstructing the excitation energy E distribution. The E resolution is ~ 500 keV, sufficient to suppress the contribution of the main feeding transitions.

These techniques will be employed in the near future with the new SPES RIB. Increased γ-ray and particle detection efficiency is required to cope with the low-intensity exotic RIB, which might be orders of magnitude less intense than in the present case.

3.4 Coulomb-excitation measurements using AGATA

The history of Coulomb-excitation measurements with AGATA dates back to the very first physics experiment with this array, which took place in April 2010 and aimed at investigation of a highly-deformed structure in ^{42}Ca [63,64] At this time, only three AGATA triple clusters were available, and scattered beam particles were detected by three position-sensitive Micro-Channel Plate (MCP) detectors of the DANTE array [59], covering angles from 105 to 142°. The measurement provided magnitudes and relative signs of numerous $E2$ matrix elements coupling the low-lying states in ^{42}Ca. The shape parameters obtained for the 0^+_2 and 2^+_2 states confirm that the excited structure possesses a strikingly large elongation, similar to that established for superdeformed bands in this mass region, and a slightly non-axial character. In contrast, those for the ground state are consistent with large fluctuations about a spherical shape. This general picture is well reproduced by state-of-the-art model calculations, although it is important to note that some discrepancies remain.

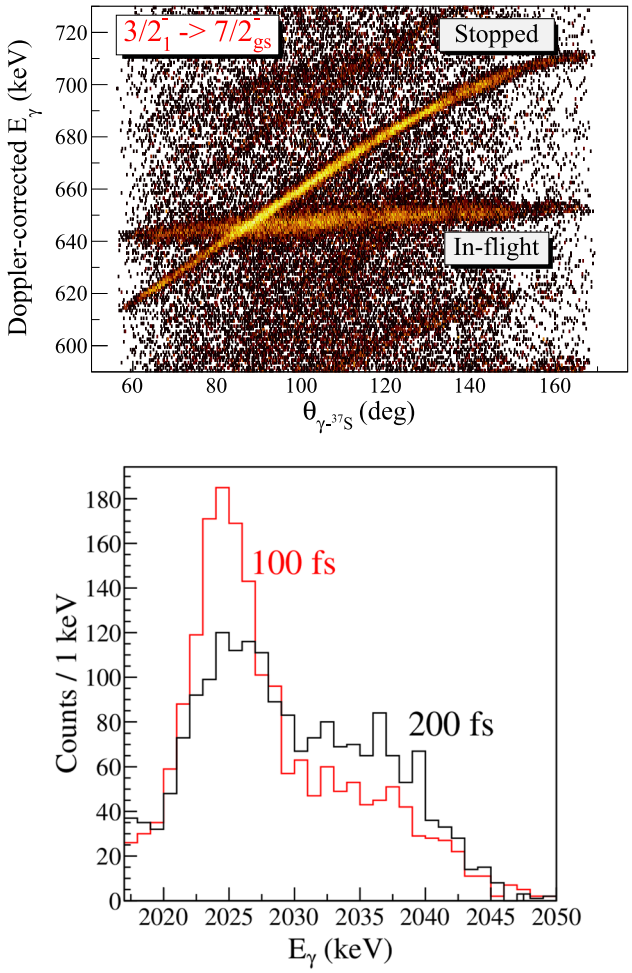

Fig. 11 (Top) Two-dimensional spectrum of the Doppler-corrected γ-ray energy of the 646-keV transition vs the angle between the γ ray and the ^{37}S recoil. The straight structure at 646 keV represents the in-flight component, the other one is associated to γ rays emitted by stopped ions. (Bottom) Simulated Doppler-corrected γ-ray energy spectra of the 2023-keV transition for two different lifetimes of the $7/2^-_2$ state

During the AGATA campaign at GANIL, Coulomb-excitation data were collected as a by-product of experiments performed at near-barrier beam energies. For example, in a fusion-fission experiment using a ^{124}Xe beam on a ^{54}Fe target [65], "safe" Coulomb excitation of the beam on a ^{nat}W target contaminant was observed, and its analysis yielded spectroscopic quadrupole moments in ^{124}Xe [66]. An ongoing analysis of slightly "unsafe" Coulomb-excitation data on ^{106}Cd, collected during an experiment aiming at lifetime measurements in ^{106,108}Sn [67], shows sensitivity to $E3$ strengths in this nucleus [68]. Both these measurements used VAMOS, covering laboratory angles around 20–30°, for particle identification.

There is strong interest in Coulomb-excitation measurements using AGATA with stable beams from the Legnaro accelerator complex, and already three such experiments

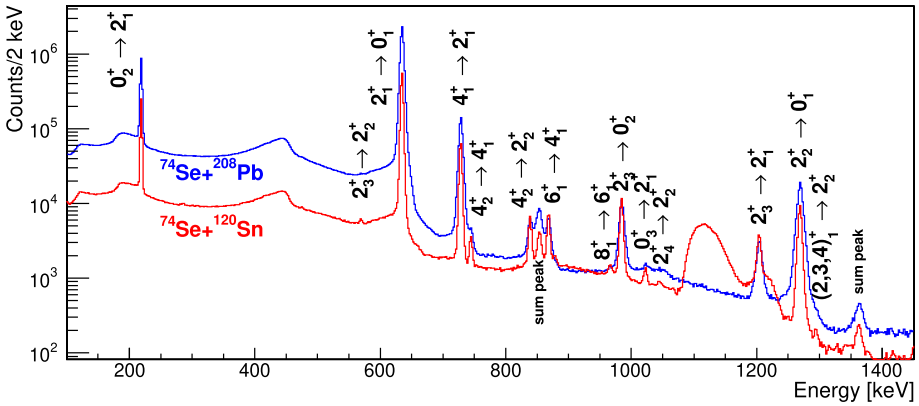

Fig. 12 Part of the spectrum of ^{74}Se, Coulomb-excited on ^{120}Sn and ^{208}Pb targets, Doppler-corrected for the projectile. The AGATA spectrometer was used for detection of γ rays in coincidence with backscattered ^{74}Se ions detected in the SPIDER array [61]. Results shown are of a quasi-online analysis of partial statistics

have been performed during the LNL campaign. They had a common focus on the shape-coexistence phenomenon, but investigated its manifestations in different regions of the nuclear chart. Several structures suspected to have different deformations were populated in ^{74}Se and ^{110}Cd, while the study of ^{96}Zr is expected to provide a precision test of the type-II shell evolution predicted by Monte-Carlo Shell Model calculations [69]. All these measurements used a modular silicon array SPIDER for particle detection. As multi-step excitation probability increases with the scattering angle, its backward configuration, covering from θ_{LAB} angles between 124° and 161°, provides an enhanced sensitivity to higher-order effects in Coulomb excitation, such as spectroscopic quadrupole moments and relative signs of electromagnetic matrix elements.

Figure 12 presents a partial spectrum resulting from Coulomb excitation of a ^{74}Se beam on ^{120}Sn and ^{208}Pb targets. The obtained energy resolution after Doppler correction is improved with respect to earlier Coulomb-excitation studies with GALILEO [70,71] and the Compton background is decreased, resulting in a clear observation of weak transitions such as $8_1^+ \rightarrow 6_1^+$, and in particular $2_3^+ \rightarrow 2_2^+$.

4 Outlook to exploit AGATA capabilities

In the near future it is anticipated that the AGATA spectrometer will be deployed with cutting-edge instrumentation, like for example GRIT (see sect 4.4) in its ultimate configuration, to take advantage of the new RIBs delivered at the second generation ISOL facility SPES. The sensitivity of the joint setup will be of the utmost importance to detect the feeble signals of exotic systems and it will be further boosted by the availability of dense and pure cryogenic or jet targets as discussed in the following paragraphs.

In multiple-step Coulomb excitation the unrivalled resolving power will permit the observation of weak transitions via multiple-coincidence measurements. Such weak decay branches may have important influence on the excitation process, and their determination will enable correct description of second-order processes in Coulomb-excitation, thus increasing sensitivity to spectroscopic quadrupole moments of excited states. In transfer reactions, the joint sensitivity of γ-ray, particle and (as required) ion chamber detectors will ensure the use of triple coincidences even with rare low-intensity RIBs. In lifetime measurements, the angular resolution of the tracking array, paired with highly-segmented complimentary detectors, will reduce the statistical uncertainties by means of the enhanced sensitivity; in addition, the opportunity to constrain the entry level in the excitation energy of the system will minimise the influence of higher lying states in the lifetime determination.

4.1 New cryogenic, jet, *jelly* targets

The weak intensity of re-accelerated unstable beams needs thick light targets to achieve sufficient luminosity for particle and γ-ray spectroscopy following direct transfer reactions. As an example, considering a beam intensity of 10^4 pps and a reaction cross section of 1 mb, a target thickness of 10^{20} at/cm^2 would be required to achieve about 100 particle-γ-ray coincidences in ten days of beam time.

A gas target at cryogenic temperatures can provide the necessary density while keeping the small dimensions compatible with the AGATA-GRIT experimental setup. The CTADIR project, financed by the Italian National call PRIN2017 for funding, aims at building a ^{3,4}He target operating at 9 K and 1 atm pressure [72]. The cylindrical target cell has a diameter of 1 cm, a thickness of 4 mm and is confined by two Havar windows, which can be made as thin as 2 μm. The target body is aluminum to minimize γ-ray absorption and the cryogenic source is provided by a Gifford McMahon device with a 2 W cooling power at 4 K in its second stage. The connection between the cryocooler second stage and the target body is assured by a copper cold finger adapted to be compatible with the GRIT geometry. Densities as high as $4 - 5 \cdot 10^{20}$ at/cm^2 can be achieved.

It is also proposed the use of the CHyMENE semisolid ^{1,2}H target [73], which is a windowless target made of a 50-100μm hydrogen film extruded into the reaction chamber, with densities around $2 \cdot 10^{20}$at/cm^2.

When using stable beams, or very intense unstable beams, above 10^7 pps, a gas jet target can also be considered. The SUGAR target [74] can reach a thickness of 10^{18}at/cm^2 and is planned to be used with AGATA with stable beams in the framework of the second LNL campaign.

4.2 Lifetimes as a key new feature

Lifetime measurements are key to access the properties of the quantum mesoscopic system that is the atomic nucleus. The decay probability from excited states is directly related to the reduced transition probability that links the initial and final state via the electromagnetic operator. For low-to-moderate product velocities known with sufficiently low uncertainties, the leading factor in the sensitivity to lifetime measurement is the angular resolution of the gamma-ray spectrometer, either for RDDS or DSAM technique covering time ranges from a few hundreds of ps down to below 1 fs. This is shown in Fig. 13 where the continuous angular measurement led to an unprecedented sensitivity. The opportunities opened up by using AGATA at the second generation ISOL facilities (SPES,HIE-ISOLDE, etc.), promising a leap in the purity, intensity and energy, will be of great impact. Striking examples are the proposed measurements of yrast and yrare states in light nuclei, presently a playground for new ab-initio theories moving from QCD EFT, that are relevant for nuclear physics and astrophysics investigations. In the nuclei at or nearby shell closures in the heavy $N = 50$ or 82 neutron-rich regions, lifetime measurements will pair with single or few-nucleon transfer-reaction cross sections to probe the single particle nature of the relevant excited states.

4.3 Future Coulomb-excitation studies with AGATA at Legnaro National Laboratories

Coulomb excitation is likely to become one of the pillars of the AGATA campaign with exotic beams from the SPES facility. For these studies, SPIDER will be installed in the forward hemisphere. As the total Coulomb-excitation cross section is given by the product of the excitation probability and the Rutherford cross section, it is necessary to make use of the important enhancement of the latter at forward scattering angles in order to maximise the counting rates with RIBs, even though lower multi-step excitation cross sections are expected in this configuration.

Possible physics cases are explored e.g. in Ref. [76]. A region of particular interest will be the neutron-rich Kr and Rb nuclei, expected to be produced at SPES with intensities considerably higher than those currently available at other

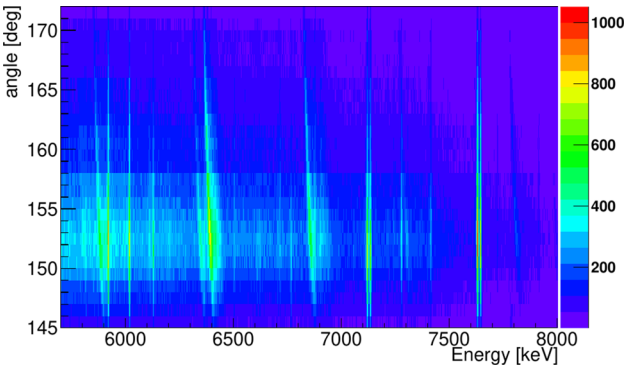

Fig. 13 Matrix of the γ-ray energy vs θ of the first interaction point for the reaction ^{14}N(d,n)^{15}O. Angular position of the first interaction point θ, with respect to the beam direction, sorted as a function of the energy of the reconstructed γ ray. The narrow straight lines correspond to the emission at rest from the AmBe(Fe) source, while the broad "tilted" lines are gamma rays emitted while the excited nucleus is moving in the Au layer. Figure adapted from Ref. [75]

European RIB facilities. These studies will search for signatures of configuration inversion and shape coexistence near $N = 60$ via detailed measurements of transition probabilities and spectroscopic quadrupole moments. Moreover, investigations of the role of triaxiality in heavy Se and Ge nuclei in the vicinity of the $N = 50$ shell closure will provide important benchmarks for beyond-mean-field and large-scale shell-model (LSSM) calculations.

In the longer term, it is anticipated that Coulomb excitation at energies around 150 MeV per nucleon will play an important role in the future AGATA campaign at FAIR. This would involve studies of the evolution of quadrupole and octupole collectivity in the regions around the doubly-magic ^{132}Sn and ^{208}Pb nuclei, as well as in the regions of rapidly changing nuclear shapes and shape coexistence, for example around $Z = 70 - 76$ or $N = 60$ [76].

4.4 GRIT outline design and capabilities

Generally for direct reaction studies with low-energy ISOL beams, the main observables to be measured are the excitation energies of the populated states, and the corresponding differential cross-sections (angular distributions). Inverse kinematics experiments consist in measuring the light recoiling particle produced by reactions between an radioactive beam particle and a light target (p, d, t, ^{4}He,…). The above observables can be deduced from the kinetic energy and scattering angle of the recoiling particle. The detection in coincidence of γ rays emitted in the decay of the populated states of interest allows a large gain, typically a factor 100 with AGATA, in excitation energy resolution, while allowing γ-ray spectroscopy measurements (e.g. lifetime and polarisation measurements) which give access to additional nuclear structure information. Obviously, such particle-γ

coincidence measurements pose a great deal of integration constraints for the particle detector at play. The GRIT European collaboration has proposed to build a new silicon detector array for optimal study of direct reactions at the European nuclear physics facilities. This new device consists of a new type of compact, high granularity, 4π acceptance Silicon array, with new digital electronics allowing seamless integration inside AGATA, as well as in the PARIS scintillator detector [77]. GRIT is a portable device for campaigns at various facilities (GANIL, SPES, ISOLDE, FAIR) in combination with AGATA or other gamma-ray detectors (PARIS, EXOGAM, GALILEO, …).

The conceptual design of the device has been driven by the aspiration towards a 4π angular coverage in both particles and gamma-ray detection. The current assembly for the detector, see Fig. 14, is a conical-shaped set of 8 trapezoidal telescopes in both the forward and backward hemispheres with respect to the beam direction, assembled with a ring of squared-shape two-layer silicon telescopes around 90 degrees. The 4π solid angle coverage is achieved with the help of annular detectors as end caps to cover the most backward and forward angles. These latter detectors will be designed so as to cope with both the ISOL beams as well as slowed down in-flight beams produced by FAIR at GSI or RIBF at RIKEN. The outer diameter of the device including its frontend electronics and dedicated reaction chamber will be compatible with mounting inside AGATA. Custom developments of digital electronics, featuring a 200 MHz sampling rate, will allow particle identification from pulse shape analysis (PSA). In a longer term, the pursuit of an R&D program to extend the capability of particle identification of the GRIT array via PSA [78–83] embedded in the electronics is desirable. In this view, the use of advanced algorithms, AI [84], firmware and computing hardware, such as GPU, could be used to accelerate and make more efficient the analysis of PSA based discrimination.

4.5 Future campaigns with GRIT

The first experimental campaigns with the ultimate GRIT setup are planned to be held with the new RIB delivered by the SPES accelerator facility at LNL. As a point of reference, SPES will deliver ^{132}Sn at 10 MeV/u, with an expected beam rate of 3.10^7 pps, ideal for direct reaction studies. The coupling of GRIT and AGATA is well advanced; see Fig. 15. A zero-degree detection system for the measurement of the heavy residues is currently being developed at LNL. The new beams delivered by SPES using UCx primary target are fission fragments and the region of the doubly-magic ^{132}Sn is illustrative of the physics program envisioned by the GRIT collaboration. In this region of the nuclide chart, the measurement of one- and two-neutron transfer reactions is proposed for investigating the shell structure around

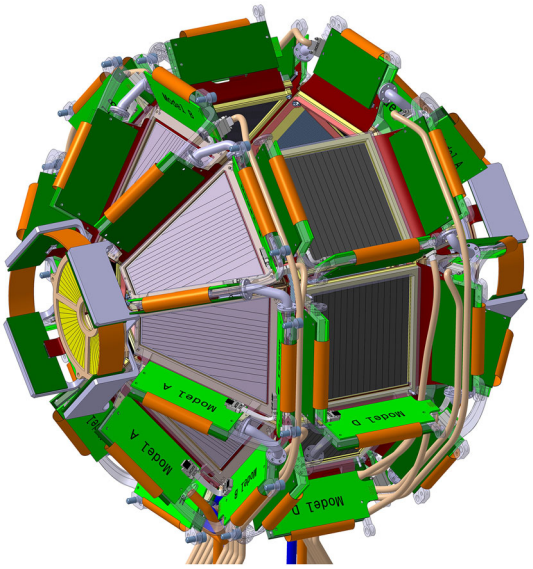

Fig. 14 CAD drawing of the ultimate GRIT array. Annular, trapezoidal and square detectors can be seen from left to right, together with the cooling blocks, green in figure. GRIT is designed so that it can be mounted inside the AGATA array (see Fig. 15)

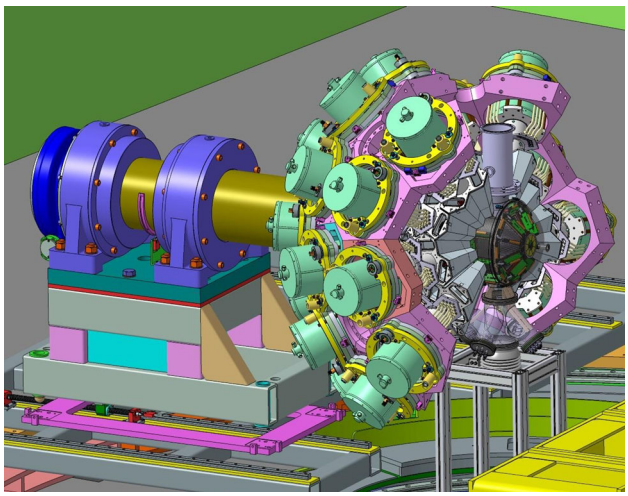

Fig. 15 CAD drawing of the provisional configuration of AGATA and GRIT at LNL. The GRIT particle array is visible in the centre of the figure and it is surrounded by the AGATA spectrometer. As discussed in the text, a cryogenic target is also compatible with the setup and, in the figure, it is inserted vertically above GRIT

$N = 132$, and its consequences for the r-process (case of low-spin orbitals). A simulation can be seen in Fig. 16, where the four panels show the angular distributions for the low-lying states populated in the reaction ^{132}Sn(d, p) for a $\Delta\ell$ = 1, 3, unitary spectroscopic factor and typical SPES intensity. For comparison with the existing experimental data see Ref. [85].

The versatility of GRIT in terms of targets will be beneficial. In addition to the standard CH_2 and CD_2 targets (commonly used for (d, p) and (p, d)…studies), triton targets can be exploited. The use of ^{3}He, ^{4}He targets (such

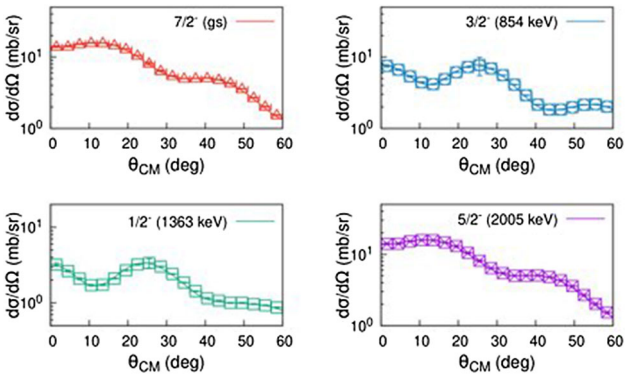

Fig. 16 Simulated angular distribution for the low-lying states considering GRIT at SPES for the reaction ^{132}Sn(d, p)

as the cryogenic CTADIR system described in Sect. 3.2.3) will allow probing of proton shells using the (^{3}He, d) and (t, ^{4}He) reactions which add and strip protons, respectively. High-momentum proton and neutron orbitals can be investigated in turn by means of the (^{3}He, ^{4}He) owing to the well-established selectivity of the He probe for high-ℓ transfer. Finally cluster transfer studies will make use of ^{7}Li foils. Also in the $N = 132$ region, neutron-neutron pairing in neutron-rich nuclei, of relevance for the time evolution of neutron stars, is planned to be investigated using the (t, p) reaction. The microscopic structure of the pygmy dipole states can be probed by (d, pγ) measurements using the PARIS array for an efficient detection of high-energy γ-rays in coincidence with recoiling protons.

5 Summary and conclusions

In the last decade, significant experimental improvements in γ-ray spectroscopy, namely the γ-ray tracking, led to a large increase in measurement sensitivity. Such sensitivity can be further heightened by coupling γ-ray spectrometers to other detectors that record complementary reaction products such as light-charged particles for transfer reactions and scattered ions for Coulomb excitation measurements.

In this paper, selected examples have been presented highlighting the power of these types of experiments when γ-ray observation is included. Results achieved before the advent of γ-ray tracking are discussed and compared with more recent experiments that have successfully exploited γ-ray tracking, in particular, with AGATA. The outlook for experiments using newly developed devices such as GRIT and other detectors such as SPIDER was also described.

In conclusion, the advent of γ-ray tracking spectrometers, such as AGATA and GRETA, together with the coupling to other auxiliary detectors greatly improved the capability to measure tinier and tinier cross sections in rare nuclear physics systems. Such opportunity is opening a new era of precision measurements at the current stable and radioactive beam facilities operating world-wide. This could provide, jointly to theoretical progresses boosted by new computational approaches, high-power and quantum computing among all, a coherent comprehension that extends from finite nuclear systems to nuclear matter and, ultimately, stars and galaxies.

Acknowledgements The authors are grateful to the AGATA, GRIT and VAMOS collaborations for having provided the material presented in this article and for the useful discussions. The authors acknowledge CERN, GANIL, LNL, TRIUMF Laboratories for having supported the experiments described in this paper. AG acknowledged the support of the Italian Ministry of University and Research (MUR) under the project CTADIR number "PRIN_2017P8KMFT". WNC was supported by STFC under grant ST/V001108/1.

Funding Information Open access funding provided by Universitá degli Studi di Padova within the CRUI-CARE Agreement.

Data availability statement This manuscript has no associated data or the data will not be deposited. [Authors' comment: The preliminary data presented in the manuscript are being fully analyzed for dedicated publications. Thereafter, data will be made available in the form and time that the different collaborations agreed.]

References

1. A. Akkoyun et al., Nucl. Instrum. Methods A **668**, 26 (2012). https://doi.org/10.1016/j.nima.2011.11.081
2. K. Kumar, Phys. Rev. Lett. **28**, 249 (1972). https://doi.org/10.1103/PhysRevLett.28.249
3. D. Cline, Annu. Rev. Nucl. Part. Sci. **36**(1), 683 (1986). https://doi.org/10.1146/annurev.ns.36.120186.003343
4. J. Simpson et al., Acta Phys. Hung. New Ser. Heavy Ion **11**, 159 (2000)
5. J. Eberth et al., Prog. Part. Nucl. Phys. **46**(1), 389 (2001). https://doi.org/10.1016/S0146-6410(01)00145-4
6. M. Schumaker et al., Nucl. Instrum. Methods A **570**(3), 437 (2007). https://doi.org/10.1016/j.nima.2006.10.185
7. M. Labiche et al., Nucl. Instrum. Methods A **614**, 439 (2010). https://doi.org/10.1016/j.nima.2010.01.009
8. W.N. Catford et al., AIP Conf. Proc. **704**(1), 185 (2004). https://doi.org/10.1063/1.1737110

9. W.N. Catford et al., Phys. Rev. Lett. **104**, 192501 (2010). https://doi.org/10.1103/PhysRevLett.104.192501
10. A. Villari, Nucl. Phys. A **693**(1), 465 (2001). https://doi.org/10.1016/S0375-9474(01)01107-1
11. P. Jardin et al., NIMB **376**, 64 (2016). https://doi.org/10.1016/j.nimb.2019.05.070
12. W.N. Catford et al., Proc. Carpath. Summer Sch. Phys. (2005). https://doi.org/10.48550/arXiv.0912.4022
13. M. Rejmund et al., Nucl. Instrum. Methods A **646**(1), 184 (2011). https://doi.org/10.1016/j.nima.2011.05.007
14. E. Pollacco et al., Eur. Phys. J. A **25**, 287 (2005). https://doi.org/10.1140/epjad/i2005-06-162-5
15. S.M. Brown et al., Phys. Rev. C **85**, 011302 (2012). https://doi.org/10.1103/PhysRevC.85.011302
16. A. Obertelli et al., Phys. Lett. B **633**(1), 33 (2006). https://doi.org/10.1016/j.physletb.2005.11.033
17. B. Fernández-Domínguez et al., Phys. Rev. C **84**, 011301 (2011). https://doi.org/10.1103/PhysRevC.84.011301
18. A. Remus, Ph.D. thesis, University of Paris XI Orsay (2009)
19. A. Ramus et al., Int. J. Mod. Phys. E **18**(10), 2056 (2009). https://doi.org/10.1142/S0218301309014287
20. V. Bildstein et al., Eur. Phys. J. A **48**, 85 (2012). https://doi.org/10.1140/epja/i2012-12085-6
21. K. Wimmer et al., Phys. Rev. Lett. **105**, 252501 (2010). https://doi.org/10.1103/PhysRevLett.105.252501
22. J. Diriken et al., Phys. Rev. C **91**, 054321 (2015). https://doi.org/10.1103/PhysRevC.91.054321
23. R. Orlandi et al., Phys. Lett. B **740**, 298 (2015). https://doi.org/10.1016/j.physletb.2014.12.006
24. C. Diget et al., J. Instrum. **6**(02), P02005 (2011). https://doi.org/10.1088/1748-0221/6/02/P02005
25. G. Wilson et al., Phys. Lett. B **759**, 417 (2016). https://doi.org/10.1016/j.physletb.2016.05.093
26. W. Catford et al., Acta Phys. Pol. B **46**(3), 527 (2015)
27. G. Burgunder et al., Phys. Rev. Lett. **112**, 042502 (2014). https://doi.org/10.1103/PhysRevLett.112.042502
28. M. Moukaddam et al., Acta Phys. Pol. **42**, 541 (2011). https://doi.org/10.5506/APhysPolB.42.541
29. S. Giron et al., Phys. Rev. C **95**, 035806 (2017). https://doi.org/10.1103/PhysRevC.95.035806
30. S. Ottini-Hustache et al., Nucl. Instrum. Methods A **431**(3), 476 (1999). https://doi.org/10.1016/S0168-9002(99)00380-0
31. B. Le Crom et al., Phys. Lett. B **829**, 137057 (2022). https://doi.org/10.1016/j.physletb.2022.137057
32. X. Pereira-López et al., Phys. Lett. B **811**, 135939 (2020). https://doi.org/10.1016/j.physletb.2020.135939
33. M. Stanoiu et al., Phys. Rev. C **78**, 034315 (2008). https://doi.org/10.1103/PhysRevC.78.034315
34. M. Assié et al., Nucl. Instrum. Methods A **1014**, 165743 (2021). https://doi.org/10.1016/j.nima.2021.165743
35. E. Clément et al., Nucl. Instrum. Methods A **855**, 1 (2017). https://doi.org/10.1016/j.nima.2017.02.063
36. F. Galtarossa et al., Nucl. Instrum. Methods A **1018**, 165830 (2021). https://doi.org/10.1016/j.nima.2021.165830
37. F. de Grancey et al., Phys. Lett. B (2016). https://doi.org/10.1016/j.physletb.2016.04.051
38. V. Girard-Alcindor et al., Eur. Phys. J. A **57**, 93 (2021). https://doi.org/10.1140/epja/s10050-021-00410-1
39. V. Girard-Alcindor et al., Phys. Rev. C **105**, L051301 (2022). https://doi.org/10.1103/PhysRevC.105.L051301
40. F. Haas et al., Il Nuovo Cimento A **110**, 9 (1997). https://doi.org/10.1007/BF03035936
41. M. Datar et al., Phys. Rev. Lett. (2013). https://doi.org/10.1103/PhysRevLett.111.062502
42. J. Papuga et al., Phys. Rev. C **90**, 034321 (2014). https://doi.org/10.1103/PhysRevC.90.034321
43. C. Paxman et al., to be published
44. J. Sanchez Rojo, Ph.D. thesis, University of York, UK, https://etheses.whiterose.ac.uk/30884/ (2021)
45. J.S. Rojo et al., in *National Astronomy Meeting Poster Exhibition*, vol. P381 (2021). https://ras.ac.uk/nam-2021/jennifer-sanchez-rojo
46. S. Paschalis et al., Nucl. Instrum. Methods A **709**, 44 (2013). https://doi.org/10.1016/j.nima.2013.01.009
47. S. Hallam et al., Phys. Rev. Lett. **126**, 042701 (2021). https://doi.org/10.1103/PhysRevLett.126.042701
48. D. Mengoni et al., Phys. Rev. C **82**, 024308 (2010). https://doi.org/10.1103/PhysRevC.82.024308
49. S. Calinescu et al., Phys. Rev. C **93**, 044333 (2016). https://doi.org/10.1103/PhysRevC.93.044333
50. A. Dewald et al., Prog. Part. Nucl. Phys. **67**, 786 (2012). https://doi.org/10.1016/j.ppnp.2012.03.003
51. A. Schwarzschild, E. Warburton, Annu. Rev. Nucl. Sci. **18**, 265 (1968). https://doi.org/10.1146/annurev.ns.18.120168.001405
52. T. Otsuka et al., Phys. Rev. Lett. **105**, 032501 (2010). https://doi.org/10.1103/PhysRevLett.105.032501
53. I. Zanon, Il Nuovo Cimento C **44**, 83 (2021). https://doi.org/10.1393/ncc/i2021-21083-8
54. I. Zanon, Il Nuovo Cimento C **45**, 66 (2022). https://doi.org/10.1393/ncc/i2022-22066-y
55. M. Ciemała et al., Eur. Phys. J. A **101**, 021303 (2020). https://doi.org/10.1103/PhysRevC.101.021303
56. M. Ciemała et al., Eur. Phys. J. A **57**, 156 (2021). https://doi.org/10.1140/epja/s10050-021-00451-6
57. J. Valiente Dobón et al., Nucl. Instrum. Methods A **1049**, 168040 (2023). https://doi.org/10.1016/j.nima.2023.168040
58. D. Mengoni, Jpn. Phys. Soc. Conf. Proc. **6**, 010015 (2015). https://doi.org/10.7566/JPSCP.6.010015
59. A. Gadea et al., Nucl. Instrum. Methods A **654**, 88 (2011). https://doi.org/10.1016/j.nima.2011.06.004
60. E. Caurier, F. Nowacki, A. Poves, Phys. Rev. C **90**, 014302 (2014). https://doi.org/10.1103/PhysRevC.90.014302
61. M. Rocchini et al., Nucl. Instrum. Methods A **971**, 164030 (2020). https://doi.org/10.1016/j.nima.2020.164030
62. C. Stahl et al., Comput. Phys. Commun. **214**, 174 (2017). https://doi.org/10.1016/j.cpc.2017.01.009
63. K. Hadyńska-Klęk et al., Phys. Rev. Lett. **117**, 062501 (2016). https://doi.org/10.1103/PhysRevLett.117.062501
64. K. Hadyńska-Klęk et al., Phys. Rev. C **97**, 024326 (2018). https://doi.org/10.1103/PhysRevC.97.024326
65. C. Schmitt et al., Phys. Rev. Lett. **126**, 132502 (2021). https://doi.org/10.1103/PhysRevLett.126.132502
66. E. Clément et al., Phys. Rev. C **107**, 014324 (2023). https://doi.org/10.1103/PhysRevC.107.014324
67. M. Siciliano et al., Phys. Lett. B **806**, 135474 (2020). https://doi.org/10.1016/j.physletb.2020.135474
68. D. Kalaydjieva et al., in preparation (2022)
69. T. Togashi et al., Phys. Rev. Lett. **117**, 172502 (2016). https://doi.org/10.1103/PhysRevLett.117.172502
70. A. Goasduff et al., Nucl. Instrum. Methods A **1015**, 165753 (2021). https://doi.org/10.1016/j.nima.2021.165753
71. M. Rocchini et al., Phys. Rev. C **103**, 014311 (2021). https://doi.org/10.1103/PhysRevC.103.014311
72. M. Sedlak et al., Nuovo Cimento C **45**, 1 (2022). https://doi.org/10.1393/ncc/i2022-22108-6
73. A. Gillibert et al., Eur. Phys. J. A **49**(12), 155 (2013). https://doi.org/10.1140/epja/i2013-13155-y
74. F. Favela et al., Phys. Rev. ST Accel. Beams **18**, 123502 (2015). https://doi.org/10.1103/PhysRevSTAB.18.123502
75. C. Michelagnoli, Ph.D. thesis, Università di Padova (2014)
76. W. Korten et al., Eur. Phys. J. A **56**(5), 1 (2020). https://doi.org/10.1140/epja/s10050-020-00132-w

77. A. Maj et al., Acta Phys. Pol. B **40**, 565 (2009)
78. J. Dueñas et al., Nucl. Instrum. Methods A **676**, 70 (2012). https://doi.org/10.1016/j.nima.2012.02.032
79. J. Dueñas et al., Nucl. Instrum. Methods A **714**, 48 (2013). https://doi.org/10.1016/j.nima.2013.02.032
80. D. Mengoni et al., Nucl. Instrum. Methods A **764**, 241 (2014). https://doi.org/10.1016/j.nima.2014.07.054
81. J. Dueñas et al., Nucl. Instrum. Methods A **743**, 44 (2014). https://doi.org/10.1016/j.nima.2014.01.009
82. M. Assié et al., Eur. Phys. J. A **51**, 11 (2015)
83. M. Assié et al., Nucl. Instrum. Methods A **908**, 250 (2018). https://doi.org/10.1016/j.nima.2018.08.050
84. L. Morselli et al., INFN An.Report (2018)
85. K. Jones et al., Nature (2010). https://doi.org/10.1038/nature09048